Adsorption of strontium from aqueous solution using ethyl butyl phosphonate (EBP) silica

Pepper, Sarah; Robshaw, Thomas; Amphlett, James; Ruder, Laura; Harwood, Laurence; Lee, Taek Seung; Whittle, Karl; Ogden, Mark

Progress in Nuclear Energy

DOI:
10.1016/j.pnucene.2024.105458

Published: 01/12/2024

Publisher's PDF, also known as Version of record

Progress in Nuclear Energy 177 (2024) 105458

Contents lists available at ScienceDirect

Progress in Nuclear Energy

journal homepage: www.elsevier.com/locate/pnucene

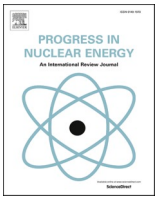

Adsorption of strontium from aqueous solution using ethyl butyl phosphonate (EBP) silica

Sarah E. Pepper [a,b], Thomas J. Robshaw [a,c,*], James T.M. Amphlett [a,d], Laura R. Ruder [a], Laurence M. Harwood [e], Taek Seung Lee [f], Karl R. Whittle [g], Mark D. Ogden [a,h]

[a] Separation and Nuclear Chemical Engineering Research (SNUCER), Department of Chemical and Biological Engineering, University of Sheffield, Sir Robert Hadfield Building, Sheffield, S1 3JD, United Kingdom
[b] Department of Materials Science and Engineering, University of Sheffield, Sheffield, United Kingdom
[c] Nuclear Engineering Group, School of Chemical and Process Engineering, University of Leeds, Woodhouse, Leeds, LS2 9JT, United Kingdom
[d] Seaborg Technologies, Titangade 11, 2200, Copenhagen N, Denmark
[e] Department of Chemistry, University of Reading, Reading, RG6 6AH, United Kingdom
[f] Organic and Optoelectronic Materials Laboratory, Department of Organic Materials Engineering, Chungnam National University, Daejeon, 34134, South Korea
[g] School of Engineering, University of Liverpool, Liverpool, L69 3BX, United Kingdom
[h] Nuclear Futures Institute, Bangor University, Dean Street, Bangor, Gwynedd, LL57 1UT, United Kingdom

ARTICLE INFO

Keywords:
Strontium-90
Ion-exchange
adsorption
functionalised silica
Active waste

1. Introduction

Strontium-90 (^{90}Sr) is one of the most abundant radionuclides released routinely or accidently into the environment (Steinhauser, 2014; Povinec et al., 2012). ^{90}Sr is hazardous, due to its relatively long half-life (~28.8 years) and toxicity to humans. Strontium behaves biochemically in a very similar way to calcium and therefore accumulates in bone tissue and teeth (Vajda and Kim, 2010). Furthermore, there is the potential for accumulation in the bodies of infants, due to presence in breast milk (Shagina et al., 2015). ^{90}Sr undergoes β^- decay to ^{90}Y, with a decay energy of 0.546 MeV. The daughter nuclide in turn undergoes further β^- decay where $t_{1/2} = 64$ h and $Q = 2.28$ MeV. Human exposure causes damage to bone marrow, leading to an increase risk of leukaemia (Morisawa et al., 2000). ^{90}Sr-contaminated materials are often referred to as "high-level waste" (Potera, 2011), although the descriptor is not actually dependant on the radionuclide in question and the definitions of high-, medium- and low-level radioactive waste vary between countries and institutions (Lennemann, 1978). This does however, illustrate the level of general concern in managing the fate of this isotope effectively.

The behaviour of ^{90}Sr, upon release to the environment, has been widely studied; often alongside ^{134}Cs and ^{137}Cs (Paasikallio et al., 1994; Mason et al., 2000; Pioch and Madozescande, 1995). Radiocaesium is more volatile and a greater concern for aerial release, but ^{90}Sr is often implicated in the contamination of water (Kim et al., 2018; Surman et al., 2014; Oji et al., 2009). For example, it often contaminates sediment in coastal regions and estuaries (Surman et al., 2014), as a result of controlled historical release from nuclear fuel reprocessing (Harrison et al., 2023), residue from nuclear weapon-testing (Rapaport et al., 2022), and unintentional release from nuclear accident (Paasikallio et al., 1994). ^{90}Sr was found at high activities ($\leq$29.13 mBq·L^{-1}) in Japanese coastal waters in 2013, following the 2011 Fukushima Daiichi disaster (Tazoe et al., 2019). Analysis of samples of foodcrops collected in Ukraine demonstrated that as late as 2019, the levels of ^{90}Sr in these products were above legal limits, resulting from the Chernobyl incident of 1986 (Labunska et al., 2021).

Therefore, treatment of aqueous waste streams is necessary to remove and contain ^{90}Sr to prevent and/or minimise its environmental

* Corresponding author. Nuclear Engineering Group, School of Chemical and Process Engineering, University of Leeds, Woodhouse, Leeds, LS2 9JT, United Kingdom.
E-mail address: t.j.robshaw@leeds.ac.uk (T.J. Robshaw).

https://doi.org/10.1016/j.pnucene.2024.105458
Received 15 July 2024; Received in revised form 30 August 2024; Accepted 20 September 2024
Available online 23 September 2024

release. Various techniques have been employed; including solvent extraction (Dhami et al., 2013), precipitation (Tan et al., 2010) and ion-exchange (Chiarizia et al., 1998; Dyer et al., 1999; Bortun et al., 1997). Solvent-extraction is generally the process of choice when the ion of interest is present in the target wastestream at concentrations >2 g L^{-1}. However, this is highly unlikely in environmental applications for ^{90}Sr capture. Conventional precipitation generally cannot achieve the decontamination factor (DF) required for the removal of such a hazardous species and so requires a tandem process, such as microfiltration to be effective, which adds cost and complexity (Wu et al., 2014). Ion-exchange involves contacting a contaminated feed solution with a solid material that has been modified to adsorb the species of interest. Solid materials can be modified to target problematic species and the resulting active waste can then be easily dewatered, prior to conversion to a wasteform.

The agreed United Kingdom strategy for the safe containment of nuclear waste is a deep geological facility (DGF) (Management, 2023), which is in alignment with the sector-wide goals for "Near Zero" release of radioactive effluent to the environment (Agency, 2018). As such, for any radionuclide capture process where the goal is disposal, rather than recycling, it is critical that: (a) the resulting active material is amenable to a wasteform-conversion process; (b) the active species is sufficiently concentrated to minimise the volume of generated waste (Asmussen et al., 2022). An adsorption or ion-exchange process generally achieves the second goal. However, the first is problematic; contaminated spent ion-exchange resins are a well-known 'orphan' wastestream within the industry, with the bulk of this waste currently in intermediate storage, pending treatment, which is unsustainable going forward (Doudou et al., 2013).

In a recent technical assessment of potential wasteform conversion routes for IX resins, vitrification was found to be the most promising; scoring highly in engineering, economic and environmental criteria (Guo et al., 2022). Borosilicate glass has been used to contain fission products and minor actinides remaining after reprocessing of SNF. However, the ability of glass to retain these species is an issue that continues to be explored. It is difficult to address, due to complexity of the system. Glass undergoes dissolution and irreversible transformation into more stable phases (Gin et al., 2013). The rate at which this occurs depends strongly on factors such as pH, temperature and solution composition. Additionally, the glass and the contained problematic species must be retained for geological timescales. International Simple Glass (ISG) was developed to aid the international nuclear glass community in understanding glass corrosion mechanisms and kinetics (Kaspar et al., 2019). It is a six-oxide borosilicate glass.

Although vitrification of conventional IX resins is feasible and demonstrable, a high organic content can be problematic for the vitrification process. This is because oxygen fugacities during the melt require controlling carefully; otherwise there is a risk that transition metals present in the glass could precipitate during processing (Jantzen et al., 1995). One alternative that has been rarely investigated is the use of a functionalised silica as an adsorbent matrix. This offers the advantages of (relatively) low organic content, plus chemical similarity with ISG. Silica-materials also offer advantages to the adsorption step in general, compared to polymeric materials, as they do not swell, have better resistance to organic solvents and can tolerate higher temperatures (Da'na, 2017).

Functionalised silicas are commercially available, although not at the scale of conventional polymeric resins. Such materials are generally mesoporous and good quality control is possible over pore volume distribution, as for an IX resin. The unfunctionalized silica is generally synthesised from polycondensation of alkoxysilanes and the resulting particles, possessing the correct physical characteristics is commonly reacted with a further alkoxysilane, containing a labile functional group, which becomes the basis of constructing an appropriate ligand (Vidal et al., 2012). For information on readily available starting functionalities, the reader is directed to the PhosphonicS range (https://www.phosphonics.com/shop/). Such materials have been reviewed for their capabilities in removal of metals (Da'na, 2017), and dyes (Al-Amrani et al., 2022) from water as well as desalination (Elma et al., 2012). The phosphonic acid group is an attractive target for investigation, being used extensively for the capture of various divalent cations, including Sr (Lanxess). Phosphonic acid-functionalised silica has been demonstrated for the separation of various metals relevant to the nuclear industry, including uranium (Zhou et al., 2016), americium (Zhang et al., 2014) and lanthanum (Wu et al., 2013). However, to the best of our knowledge, no such studies exist demonstrating the same for strontium.

Because Sr-90 is a significant problem in the context of spent nuclear fuel reprocessing waste treatment (Aguila et al., 2016) and also environmental remediation in the event of intentional or accidental release of radionuclides (James et al., 2019). Thus, there are a multitude of different aqueous wastestreams from which Sr removal might be desirable. As such, given the lack of existing basic data, we have chosen in this work to investigate fundamentals of aqueous adsorption behaviour of Sr, with respect to a commercially-available phosphonic acid-functionalised silica. These are the first data of this nature to be reported, as far as we are aware, and will hopefully catalyse further research in this important area.

2. Experimental

2.1. Chemical reagents and equipment

All chemicals used were analytical grade or better and purchased from Sigma-Aldrich unless stated otherwise. Ethyl/butyl phosphonate silica (EBP-Si) was purchased as the Na form directly from PhosphonicS Ltd. Prior to use, EBP-Si was converted to the protonated form by contacting with 1 M hydrochloric acid for 24 h, before washing 3 × 100 times the sample mass, with deionised water. The resulting suspension was stored under deionised water.

Stock solutions of Sr were prepared by dissolving strontium (II) nitrate in deionised water. Sr analysis was carried out using a PerkinElmer Atomic Absorption Spectrometer AAnalyst 400. Calibration was performed using a standard Sr^{2+} solution of 1000 ± 3 mg L^{-1} (Fisher Scientific) diluted with 1% nitric acid (spectroscopic grade). All analysis was performed in triplicate.

2.2. Effect of pH, metal concentration and ionic strength

The adsorption of Sr by EBP-Si as a function of pH was studied by equilibrating 1.6 mL of wet settled resin with 30 mL solution containing 100 ppm strontium (as strontium nitrate) for a period of 12–16 h. Suspensions were shaken on a mechanical shaker at ambient temperature. The pH was altered using 1.0 M solutions of hydrochloric acid or sodium hydroxide as necessary to alter the pH in the range 0.3–5. After contact, the suspension was allowed to settle under gravity, a process which took around 5 min. The pH of the solution was measured and a portion removed for dilution with 1% nitric acid prior to analysis by atomic absorption spectroscopy.

Extraction efficiency (E) and the Sr uptake capacity of the silica at equilibrium (q_e, mmol g^{-1}), were calculated as follows:

$$E\% = \left(\frac{c_0 - c_f}{c_0}\right) x\, 100\% \quad (1)$$

$$q_e = \left(\frac{c_0 - c_f}{c_f}\right) x\, \frac{V}{m} \quad (2)$$

Where c_0 and c_f represent the initial (pre-contact) and final (post-contact) concentrations, respectively, V represents the volume of solution in contact with the EBP-Si and m represents the mass of the resin. The mass of EBP-Si was calculated by converting the volume of wet settled silica, to a dry mass equivalent. This was experimentally determined by drying

5 x 10.0 mL samples of the conditioned, protonated silicas, in an air-flow oven at 80 °C, for 24 h. Accurate mass measurements were taken before and after drying, using a an analytical balance, with a precision of 0.0001 g and an average retention of mass and standard deviation were calculated. The determined adsorbent density, calculated in this way was 0.498 ± 0.007 g mL^{-1}.

The effect of ionic strength, using 2 different salts with non-competing cations, was investigated using a constant Sr(II) concentration (100 mg L^{-1}) at a set initial pH value of 3.0 ± 0.1. The ionic strength was increased from 0.010 to 2.0 M using NaCl or $(NH_4)_2SO_4$. Contact and analysis took place as previously described.

The effect of metal concentration was studied via isotherms, which were performed in a similar fashion to other equilibrium experiments. The pH was again set at 3.0 ± 0.1 and the concentration of St varied from 10 to 5000 mg L^{-1}. Contact and analysis took place as previously described. The data were fitted with the two-parameter isotherm models Langmuir (Eqn. (3)), Freundlich (Eqn. (4)), Temkin (Eqn. (5)) and Dubinin-Radushkevich (Eqn. (6)). The fitting was carried out by non-linear least-squares analysis using the SOLVER function within Microsoft Excel (Billo, 2004).

$$q_e = \frac{K_L C_e}{1 + a_L C_e} \tag{3}$$

$$q_e = \frac{RT}{b_T} ln(A_T C_e) \tag{4}$$

$$q_e = a_F C_e^{b_F} \tag{5}$$

$$q_e = q_D \exp\left(- B_D \left[RTln\left(1 + \frac{1}{C_e}\right)\right]^2\right) \tag{6}$$

For all these models, q_e denotes the equilibrium adsorbent metal ion concentration (mg·g^{-1}) and C_e is the equilibrium solution phase metal ion concentration (mg·L^{-1}). The Langmuir model describes a monolayer chemisorption processes and assumes that all binding sites are of homogeneous energy, where a_L and K_L are isotherm constants. The Dubinin-Radushkevich isotherm assumes that the energy of binding sites follows a Gaussian distribution. The B_D term is an isotherm constant and q_D is the maximum surface loading capacity, R is the universal gas constant (8.314 J mol^{-1} °K^{-1}) and T is the absolute temperature (°K). Both models have previously been used to describe the adsorption of metals by EBP silica (Pepper et al., 2018). The Freundlich isotherm is an empirical model, commonly used to describe physisorption processes, where a_F and b_F are constants. The Temkin isotherm assumes that the fall in the heat of sorption is linear rather than logarithmic, as implied in the Freundlich equation, and A_T and b_T are isotherm constants. These last two models are generally observed to be less suitable for description of metal-uptake by ion-exchange/chelation mechanisms (James et al., 2019; Bezzina et al., 2020), but are useful to include as a point of comparison.

2.3. Kinetics

Kinetic experiments were performed by contacting 20 mL wet settled resin with a 500 mL solution of Sr(II) at an initial pH value of 3.0 ± 0.1. The suspension was agitated on an orbital shaker for up to 250 min and aliquots were removed at various time intervals and analysed as described in Section 2.1. The solid to solution ratio was such that samples removed over the course of the experiment were less than 10% of the solution volume, to avoid dilution effects.

2.4. Dynamic experiments

Dynamic experiments were conducted as reverse flow experiments as follows; a 2 mL volume polypropylene column (Supelco) was filled with approximately 0.747 g of protonated EBP-Si, with a 3 mm Teflon frit at both ends. A feed solution containing 100 mg L^{-1} Sr(II) at an initial pH value of 3.0 ± 0.1 was passed through the column using a Watson Marlow 120S peristaltic pump, while the effluent was collected at regular intervals using a Bio Rad Model 2110 fraction collector. The counter-flow system is useful in laboratory-scale experiments for more unusual adsorbent matrices. Columns are typically set up with a small void space at the top of the column, to account for any changes in volume that might occur to the adsorbent bed in the process of saturation with the adsorbate. As such, presenting the inlet solution to the base of the column eliminates any disturbance of the column material that could occur (particularly at higher flow-rates), which can cause channelling and premature partial breakthrough.

The effluent fractions were analysed for Sr(II) content as described in Section 2.1. The samples were collected until the feed concentration was equal to the effluent concentration, i.e. $c_0 = c_f$, where c_0 and c_f represent the feed and effluent concentrations respectively.

The fluoride breakthrough data were fitted with the empirical Dose-Response model (Eqns. (7) and (8))

$$\frac{C}{C_i} = 1 - \frac{1}{1 + \left(\frac{V_{eff}}{b}\right)^a} \tag{7}$$

$$q_0 = \frac{bC_i}{m} \tag{8}$$

Where C is the concentration of adsorbate in the effluent at a given point, C_i is the concentration of adsorbate in the inlet stream, V_{eff} is the volume of solution eluted from the column (mL), a and b are constants of the Dose-Response model, q_0 is the theoretical maximum uptake capacity of the adsorbent material in a dynamic environment (mg g^{-1}) and m is the dry mass of silica (g).

The data were further fitted with the Adams-Bohart model (Eqn. (9)), which postulates that the adsorption behaviour is proportional to both residual capacity of the adsorbent bed and the concentration of adsorbate (Robshaw et al., 2019a).

$$\ln\left(\frac{C}{C_i}\right) = k_{AB} C_i t - \frac{k_{AB} N_0 Z}{v} \tag{9}$$

where k_{AB} = Adams-Bohart kinetic constant (mL mg^{-1} min^{-1}), t = time (min), N_0 = theoretical maximum uptake capacity of the hydrated resin (mg mL^{-1}), Z = bed depth of column (cm) and v = linear flow rate (mL min^{-1}). All other terms as previously described.

3. Results and discussion

3.1. Uptake of strontium as a function of pH, for investigation of uptake mechanism

In Fig. 1 the extraction of Sr^{2+} as a function of aqueous proton concentration is presented. The pH was measured, post-sorbent contact from 0.5 to 2.5 and the data are displayed in Fig. 1a as a function of the equilibrium pH value. Below a pH of 1, extraction efficiency is very low. However, above pH 1, the extraction increases linearly reaching a maximum value around pH 2.3, which corresponds with ~100%. The point at which 50% extraction of Sr^{2+} is achieved (pH_{50}) is calculated from linear regression and occurs at ~ pH 1.57 ± 0.05.

Fig. 1B shows log_{10} q values as a function of pH for strontium uptake by EBP-Si. As expected, the value of q increases with increasing pH. Because q_e can be measured in units of mmol g^{-1}, these log_{10} values can be plotted against equilibrium pH (-log_{10} [H^+]). A straight line gradient indicates that the number of protons exchanged per metal ion adsorbed is consistent throughout the adsorbate concentration range studied. The gradient of the graph indicates the number of protons exchanged during metal uptake. The value obtained in this case is 2.23 and corresponds approximately to the charge on the strontium ion. This might be thought

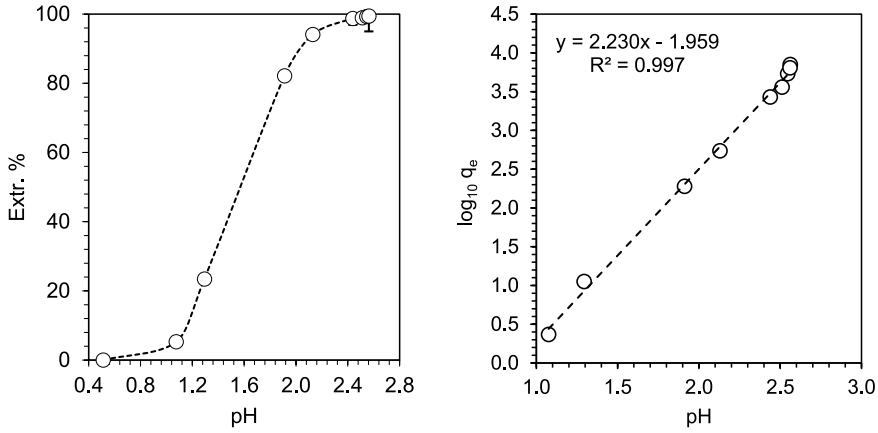

Fig. 1. Extraction of Sr by EBP silica as a function of equilibrium pH. 1.6 mL silica in 30 mL solution. [Sr] = 100 mg L^{-1}. T = 21 °C. Contact time = 24 h. A) Extraction efficiency (%), line added to aid the eye. B) $\log_{10} q_e$ slope analysis given by dashed line. Error bars represent 2 x standard deviation (approx. 95% confidence intervals) from triplicate measurements. Error bars in B are too small to be observed.

to indicate that ion exchange is likely to be the dominant mechanism in this system (exchange of two protons for one Sr^{2+} ion. However, it is known that the phosphonic acid moiety acts as a −1 ligand and can retain one proton even upon coordination with a metal ion (Robshaw, 2019). Thus, the calculated value being slightly greater than 2 more likely reflects the ability of the large Sr^{2+} ions to coordinate multiple functional groups simultaneously, when the pore environment is sufficiently sterically-crowded (Robshaw et al., 2020a). In previous experiments with this adsorbent. The experimental values returned for Co and Ni uptake were 0.94–1.32, indicating less bridging behaviour from these smaller ions (Pepper et al., 2018). In this study, experimental conditions (apart from the metals of interest) were equivalent to this work. As such, it provides the most valid point of comparison to the particulars of interaction between this specific metal and adsorbent and will be mentioned a number of times. Spectroscopic exploration of the adsorbent, post-Sr-capture (for example, X-ray photoelectron spectroscopy) would be useful in evidencing this theory.

Another objective of this experiment was to illustrate the effect of competition with protons, on Sr uptake. Other studies have demonstrated that the phosphonic acid moiety can extract Sr at hydroxide concentrations of up to 1 M (Chiarizia et al., 1998). However, basic pHs cannot be explored in this work, because of dissolution of the silica. This is an inherent limitation of the adsorbent. As such, we were cautious in only investigating an acidic and fairly limited pH range. It would be of interest in subsequent work to explore a broader pH range and to investigate the precise pH at which the adsorbent starts to hydrolyse. An adsorbent of somewhat similar functionality, ammonium molybdophosphate (AMP), was investigated for Sr affinity and found to have very different tolerances to pH, with adsorption capacity tripling, with a pH change from 6 to 8 (Park et al., 2010). This illustrates the fact that the adsorbent matrix is not a non-factor in determining the fundamental adsorption behaviour (Pepper et al., 2018; Robshaw et al., 2023).

3.2. Isotherm behaviour

The isotherm data were modelled using a variety of two parameter models to determine strontium loading behaviour (Table 1). The Langmuir model returned the highest R^2 value and thus best describes the uptake of Sr^{2+} onto the surface of EBP-Si (Fig. 2.), which implies binding site homogeneity and monolayer loading (Robshaw et al., 2019b). The monolayer saturation capacity, q_m (mg·g^{-1}), was calculated from the Langmuir equation using Eqn. (7) (see Table 1).

$$q_{max} = a_L / K_L \quad (7)$$

Table 1
Parameters return from the fitting of thermodynamic Sr uptake data to a number of two-parameter model. ± 0.1, adjusted with HCl. T = 21 °C. Contact time = 24 h.

Langmuir		Dubinin-Radushkevich	
K_L	0.062 ± 0.002	B_D (x10^{-9})	7.2 ± 0.3
a_L	125 ± 2	q_D (mg·g^{-1})	59.7 ± 0.6
q_{max} (mg·g^{-1})	43.7 ± 0.2	E (kJ·mol^{-1})	8.3 ± 0.1
R^2	0.9971	R^2	0.9909
Freundlich		**Temkin**	
b_F	0.41 ± 0.05	A_T (x 10^{+3})	3.6 ± 0.6
a_F (x 10^{-3})	1.5 ± 0.2	b_T (x 10^{+7})	3.2 ± 0.2
R^2	0.9620	R^2	0.9515

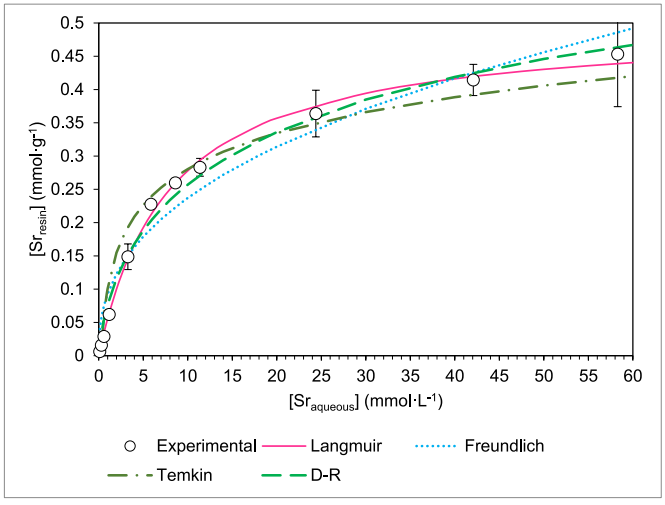

Fig. 2. Strontium loading isotherm for EBP silica. 1.6 mL silica in 30 mL solution. pH = 3.0 ± 0.1, adjusted with HCl. T = 21 °C. Contact time = 24 h. Error bars represent 2 x standard deviation (approx. 95% confidence intervals) from triplicate measurements. Some error bars are too small to be seen.

The maximum loading capacity for Sr^{2+} uptake on EBP-Si determined using the Langmuir model was 43.7 ± 0.2 mg g^{-1} (0.499 ± 0.002 mmol g^{-1}). Given the high R^2 value, this was considered to be the most accurate estimate of the adsorbent's maximal capacity and we may accept that the binding sites for EBP-Si are degenerate in nature; i.e. that

the dominant loading mechanism is the bridging of one Sr^{2+} ion across two phosphonate moieties (Fig. 1). This value is rather greater than the uptake, attained for the same adsorbent, of Cobalt and Nickel. However, there is reason to suspect in that study that the determined q_e may have continued to increase beyond the reported experimental range (Pepper et al., 2018). In comparison with adsorbents for Sr in general, the silica displays a middling capacity only. In fact, commercial ion-exchange resins are known to adsorb Sr to a capacity of >350 mg g^{-1} (Ali et al., 2020). Silica extractants are fundamentally restricted in capacity, due to the limitations of how many ligands can be bonded to the surface silanol groups per mass unit, which is observed in previous studies (Pepper et al., 2018; Robshaw et al., 2023; Sarkar et al., 1996). The advantage of the adsorbent is the retention of reasonable capacity, whilst hopefully offering superior chemical compatibility with the intended wasteform.

The Dubinin-Radushkevich (D-R) isotherm model allows for the calculation of the mean free energy of sorption (E), using Eqn. (8).

$$E = {}^{1}\Big/\sqrt{2B_D} \tag{8}$$

It is often stated in the literature that E value below 8 kJ mol^{-1} corresponds to a physisorption uptake mechanism, whereas values above 8 kJ mol^{-1} correspond to a chemisorption, or ion-exchange uptake mechanism (Pepper et al., 2018; Ogden et al., 2017). Although the D-R model does not describe uptake behaviour quite as well as the Langmuir model, the mean free energy of sorption value obtained (Table 1) would suggest chemisorption, consistent with the expected uptake mechanism here. The value of 8.3 ± 0.1 kJ mol^{-1} is nonetheless rather lower than that exhibited for other adsorbents for Sr uptake. For example, a sulfonic acid-functionalised hypercrosslinked polymer recorded a value of 18.2 ± 1.3 kJ mol^{-1} (James et al., 2019). This supports the point made in 3.1. regarding the adsorbent matrix effect. However, the adsorption affinity is stronger than for inorganic adsorbents with non-chelating functionality. A number of metal oxide/hydroxide materials were studied for Sr uptake, with the recorded E values being ~4–6 kJ mol^{-1} (Bezhin et al., 2021). We were unable to find any examples in the literature of application of the D-R isotherm to the adsorption of Sr onto a phosphonic acid-functionalised resin, for a more direct comparison. The closest example was a graphene oxide material, functionalised with aminomethylphosphonic acid groups (Alamdarlo et al., 2021). These experiments yielded E values of 5.5–6.1 kJ mol^{-1}; lower than for our work. The binding was also stronger than for Co and Ni, using the same adsorbent (7.2–7.6 kJ mol^{-1}) (Pepper et al., 2018). This supports the theory that Sr_{2+} ions bridge between two phosphonate groups and are therefore chelated more strongly.

The maximum loading capacity predicted from the D-R isotherm model is 59.7 ± 0.6 mg g^{-1} which is approximately 30% greater than the value predicted by the Langmuir model. Because the D-R model accounts for surface heterogeneity, it allows for weaker adsorption sites to become occupied by adsorbate ions, at higher adsorbate concentrations, therefore increasing the maximum uptake capacity. As such the q_D values calculated by this model are generally higher than the equivalent Langmuir q_{max} values. Previous application of the D-R isotherm model has given q_D predictions far in excess of the Langmuir model (Ogden et al., 2017; Robshaw et al., 2020b).

The Freundlich and Temkin correlation coefficients demonstrate poorer model fits than Langmuir and D-R, which is expected, as multilayer adsorption would not be predicted for this adsorbent. The Freundlich model parameter of $1/b_F$ which can be correlated to adsorption intensity is 2.44 ± 0.05 which is indicative of a favourable absorption process (Bezzina et al., 2020).

It is notable that the Langmuir model provides the best description of the adsorption process in this case; whereas in most previous studies of ion adsorption via chelating polymeric resins, the D-R model is usually superior (Ogden et al., 2017; Barton et al., 2019; Amphlett et al., 2018a). This is possibly because of the lower extent of functionalisation that is achievable with a silica matrix (Pepper et al., 2018). Ion-exchange resins, while enjoying better capacity, tend to exhibit more steric crowding of functional groups. This leads to non-degenerate binding sites, as adsorbate ions can become coordinated to multiple ligands (Robshaw et al., 2019b, 2020a). As such, the D-R model provides a better fit to the data, as it accounts for surface heterogeneity.

3.3. Effect of ionic strength

The effects of varying ionic strength, from 0 to 2 mol L^{-1}, on Sr adsorption are shown in Fig. 3. As expected, increasing ionic strength decreases the amount of Sr uptaken and it is well known that, as a general principle, increasing ionic strength has a negative effect on the distribution coefficients for alkali earth metals achievable by resins which operate via chelation (Luttrell et al., 1971). It can be seen than Cl^- has a markedly greater suppressive effect than SO_4^{2-}. It is mentioned in technical publications that elevated Cl^- is known to slightly decrease the selectivity of AMPA resins, though no explanation is given for this behaviour (Meyers, 1998).

The formation constants for the aqueous complexes $SrCl^+$ and $SrSO_4$ are similarly small, having been determined as 2.73 (Hasegawa et al., 1967) and 5.25 (Arcis et al., 2014). The lesser effect of addition of SO_4 may be due to precipitation on the silica surface, because $SrSO_4$ is only sparingly soluble in water (~125 mg L^{-1} at ambient temperature. It is known that the presence of an adsorbent surface can promote precipitation of adsorbate salt on the surface, due to an increase in potential nucleation sites (Robshaw et al., 2020b).

Should be noted that the adsorbent was operating here at a lower pH than is recommended industrially for the phosphonic acid group to retain its selectivity (Meyers, 1998). The adsorption was intentionally being tested here under aggressive conditions, which would test its limits. It is notable that the adsorption is still significant at a [Cl] equivalent to that of seawater (~19 g L^{-1}).

3.4. Kinetics

The kinetic experiment (Fig. 4) illustrates that the Sr uptake by EBP silica is very rapid, with >99% metal extraction complete within 1 h. We observed similar rapidity when the same material was assessed for Co and Ni removal (Pepper et al., 2018). In contrast, a more conventional phosphonic acid-bearing polymeric resin did not achieve equilibrium update of SR within the experimental timeframe of 1 h (Chiarizia et al., 1998), while an AMPA-functionalised graphene oxide achieved

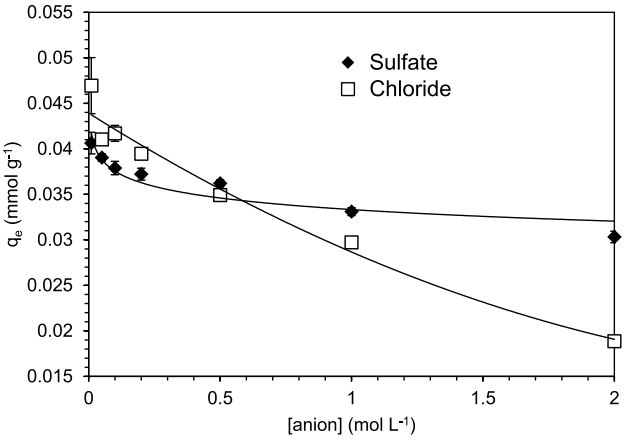

Fig. 3. Effect of increasing ionic strength, using NaCl and $(NH_4)_2SO_4$, on Sr adsorption by EBP silica. [Sr] = 100 mg L^{-1} pH = 3.0 ± 0.1 again. T = 21 °C. Contact time = 24 h. Trendlines included to guide the eye. Error bars represent 2 x standard deviation (approx. 95% confidence intervals) from triplicate measurements. Some error bars are too small to be seen.

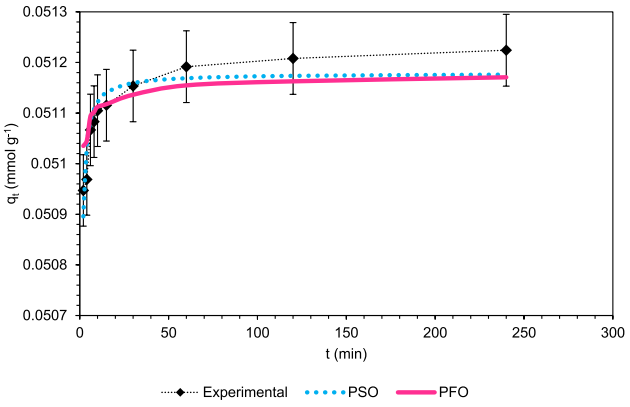

Fig. 4. Adsorption of Sr by EBP silica over time, with attempted modelling, using the pseudo-first-order (PFO) and pseudo-second-order (PSO) rate equations. 10 mL silica in initial volume of 500 mL solution. [Sr] = 100 mg L^{-1}. T = 21 °C. Contact time = 250 min.

equilibrium in ~30 min (Alamdarlo et al., 2021). Also displaying rapid kinetics (equilibrium in <40 min) was a resin impregnated with Di-(2-ethylhexyl) phosphoric acid (Kalal et al., 2017). Where modelling was attempted, in all these studies, it was found the PSO model gave a better description of the data (Table 2). Clearly the phosphonic acid functionality is not the only influential factor in kinetic behaviour. It is well-known that the process of adsorption onto a porous medium follows 5 discrete stages: 1st, transport of the adsorbate from bulk solution to particle surface, 2nd, diffusion through the stagnant aqueous film surrounding the adsorbent particle, 3rd, diffusion through the intra-particular water contained in the adsorbent pores, 4th, chemical reaction upon the surface, 5th, transport of the exchanged species away from the surface. Any one of these stages may be rate-limiting for the adsorption kinetics, and can dominate at different times during adsorption (Harland, 1994). As such, when the kinetics are not chemical reaction-controlled, it is significant whether the adsorbent is surface, or pore-functionalised, and the hydrophobicity of the adsorbent matrix. For this reason, as a review has stated (Tran et al., 2017), it is unwise to infer that agreement with the PSO model means that the adsorption kinetics are dependent on the chemical reaction of the adsorption (Ali et al., 2015). In this instance, the PSO model provided a superior fit to the data, with the PFO model substantially over-estimating the equilibrium adsorption capacity of the silica.

3.5. Dynamic experiments

Dynamic experimental data are shown in Fig. 5, with the calculated parameters seen in Table 3. The column efficiency % was calculated with reference to the Langmuir q_{max} value from the isothermal experiments.

At both flow rates, the breakthrough does not entirely follow the expected sinusoidal curve and behaviour is slightly non-ideal (Fig. 5). In both cases, breakthrough begins at ~150 min and approaches a C_0/C_t value of 1. This happens much more rapidly at a faster flow rate of 12 rpm and a value of ~0.95 is reached, whereas for the flow rate of 6 rpm,

Table 2
Calculated parameters from the fitting of kinetic data from Fig. 4 to the pseudo-first-order and pseudo-second-order models.

Calculated parameter	Lagergren PFO model	Blanchard PSO model
q_e (mg·g^{-1})	70.4 ± 16.4	51.2 ± 1.7
k_1 or k_2	25.3 ± 12.1	1760 ± 280
$t_{1/2}$ (min)	0.561 ± 0.298	0.0111 ± 0.0017
h_0 (mg·g^{-1}·min^{-1})	0.126 ± 0.073	4.61 ± 0.72
R^2	0.972	0.990

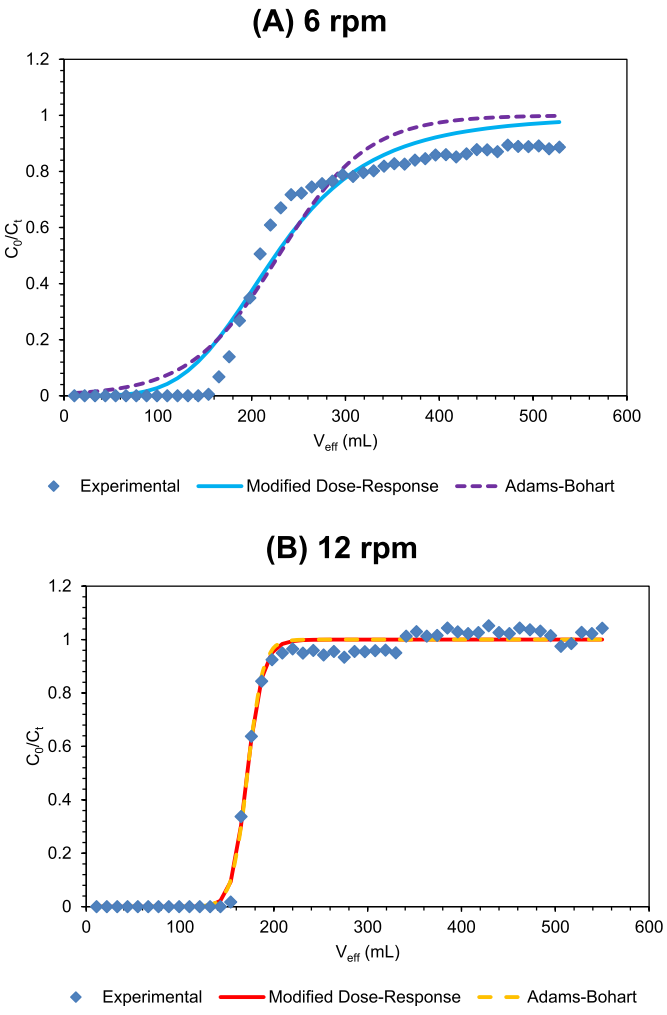

Fig. 5. Dynamic Sr breakthrough curves for an EBP silica column, run at 2 different flow-rates. Column volume = 2 mL. Column mass = 0.747 g [Sr] = 100 mg L^{-1} pH = 3.0 ± 0.1.

Table 3
Calculated operating parameters from the breakthrough curve experiments, with conditions as per Fig. 5.

	6 rpm	12 rpm
Modified Dose-Response Model		
a	4.36 ± 0.37	20.8 ± 2.0
b	225 ± 5	172 ± 1
q_0 (mg·g^{-1})	31.6 ± 0.7	24.1 ± 0.1
Column efficiency (%)	72.3	55.1
R^2	0.934	0.963
Adams-Bohart Model		
k_{AB} (mL·g^{-1}·min^{-1})	3.26 ± 0.40	36.0 ± 3.7
q_0 (mg·g^{-1})	32.1 ± 0.8	25.2 ± 0.002
Column efficiency (%)	73.5	57.7
R^2	0.905	0.961

breakthrough reaches only ~0.75, followed by a more gradual increase of Sr effluent concentration. A two-stage breakthrough, or non-linear breakthrough is often indicative of binding site heterogeneity, whereby the experiment reaches a stage where weaker sites are not fully saturated, but partial breakthrough occurs, due to their low affinity for the target ion; though this is more common in systems with more complex solution chemistry, where competitive and/or cooperative adsorption takes place (Robshaw et al., 2020c, 2021). The fact that the isothermal data follows the D-R isotherm supports the case for some

surface heterogeneity.

As noted, breakthrough does not begin at a significantly different effluent volume when the flow rate is increased. However, because breakthrough is slower at 6 rpm, the calculated q_0 values for the adsorbent are greater. Despite this, in an engineering application, the column would most likely be taken offline after the early stages of breakthrough (Harland, 1994), so there would be little practical benefit to running at a lower rpm and it would be more advantageous in practice to run at higher rpm and take the benefit of being able to treat a greater volume of water per time unit.

In common with a number of previous studies (Robshaw et al., 2019a; Barton et al., 2019; Amphlett et al., 2018b), the MDR model is superior in describing the breakthrough behaviour. The MDR is an empirical model and no fundamental assumptions can be drawn from the agreement of a dataset to this model. It is chiefly valued for is its ability to minimise deviations between the sinusoidal curve generated and experimental data (Robshaw et al., 2020c; Tavakoli et al., 2013). The Adams Bohart model assumes that the probability of successful adsorption is dependent on both the concentration of binding sites available and the concentration of adsorbate flowing through the column (i.e. a pseudo second-order reaction) (Robshaw et al., 2019a). The agreement of the data with this model supports the findings in static kinetic experiments. The difference in quality of model fit is negligible for the 12 rpm experiments, but significant at 6 rpm (Table 3).

Comparing dynamic q_0 values with column efficiency, it is clear that the dynamic values are significantly lower, though still appreciable. This is again common in dynamic experiments, where the adsorption process does not reach equilibrium (Robshaw et al., 2020b), although, when dealing with strong adsorption interactions, the two values have been seen to be equivalent, or nearly equivalent, as the uptake is sufficiently rapid for equilibrium to be reached in the active zone of the column. This has been observed specifically in the case of Sr adsorption (Khanchi et al., 2007).

3.6. Overall performance of the adsorbent

Table 4 shows how the thermodynamic and kinetic key variables obtained in these experiments compare with other adsorbents reported previously. The dynamic performance could not be compared, as modelling of dynamic adsorption appears not to be commonly performed in the literature, for reasons that are unclear. It can be seen that EBP silica exhibits moderate performance in terms of both capacity and kinetics. However, it must be remembered that this adsorbent has unique capabilities in terms of synergy with a viable final wasteform, which can be applied specifically to an active waste remit (Gin et al., 2013; Kaspar et al., 2019). This capability would be the lynchpin of a viable engineering process and thus, even with modest thermodynamic and kinetic performance, it is likely that EBP silica would be progressed in a sorbent-screening scenario, over adsorbents which have a less feasible, or less certain, pathway to a final disposal route (Atkinson et al., in press).

Most sources pertaining to vitrification of active waste are concerned with the % mass loading of the spent adsorbent material as a whole, rather than the % mass loading of the contaminant of interest. Rather, the dose contribution of the active species present is more important (Cicero-Herman et al., 1998). A reasonable total waste % mass loading for vitrification is considered to be 25–50 (Atkinson et al., in press). However, this is based on vitrification of organic resins, for which there is a considerable difference ($\leq$68%) in the mass of waste going in to the process, verses the mass present in the actual wasteform (Cicero-Herman et al., 1998). Glass wasteforms have been produced, which incorporate $\leq$28% mass Sr-90 (Strachan and Schulz, 1977), but it was accepted that the activity level of this wasteform was too high and generated too much thermal energy to be viable for long-term storage. These challenges must be addressed in ongoing work.

4. Conclusions

Silica-based materials as a Sr-capture medium merit investigation, due to their potential synergy with a number of wasteform routes. We have, for the first time, made a systematic investigation of fundamental Sr adsorption parameters, using a chemically-modified silica, with ethyl/butylphosphonic acid functional groups. The silica exhibited a moderate maximal uptake capacity of 43.7 $\pm$ 0.2 mg g^{-1}, which was nonetheless rather greater than the capacity of the same material for transition metals. The Langmuir isotherm was the most appropriate model for describing the uptake, although the Dubinin-Radushkevich model was also acceptable. The uptake was determined, almost certainly, to proceed via ion-exchange. Kinetics were rapid, with near equilibrium reached in ~60 min. Pseudo-second-order kinetic behaviour was observed. In dynamic experiments, the adsorbent tolerated a fairly rapid inlet flow-rate of 12 rpm, with ~55% retention of capacity and breakthrough could be well-described via the modified dose-response model. Future work will focus first on the adsorbent's ability to remove Sr from accurately-simulated industrial wastewater, then on conversion of Sr-loaded silica into stable vitreous or alternate wasteforms and the testing of their physical and chemical integrity.

CRediT authorship contribution statement

Sarah E. Pepper: Writing – original draft, Project administration, Methodology, Investigation, Funding acquisition, Formal analysis, Conceptualization. **Thomas J. Robshaw:** Writing – review & editing, Writing – original draft, Investigation. **James T.M. Amphlett:** Writing – original draft, Formal analysis. **Laura R. Ruder:** Methodology, Formal analysis. **Laurence M. Harwood:** Supervision, Funding acquisition, Conceptualization. **Taek Seung Lee:** Funding acquisition, Conceptualization. **Karl R. Whittle:** Funding acquisition, Conceptualization. **Mark D. Ogden:** Writing – review & editing, Writing – original draft, Supervision, Resources, Project administration, Funding acquisition, Data curation, Conceptualization.

Declaration of competing interest

The authors declare that they have no known competing financial interests or personal relationships that could have appeared to influence the work reported in this paper.

Table 4
Comparison of Removal of Sr from solution between EBP silica and other notable adsorbents reported in the literature.

Adsorbent	Sr capacity- static (mg·g^{-1})	Equilibration time (min)	Reference
EBP silica (this study)	43.7 $\pm$ 0.2	60	(this study)
(aminomethyl) phosphonic acid-graphene oxide	142.4	30	Alamdarlo et al. (2021)
Crown ether-functionalised ion-exchange resin	7.7 $\pm$ 0.4	30	Surman et al. (2014)
Sulfonic acid-functionalised hypercrosslinked polymer	95.6 $\pm$ 2.8	1	James et al. (2019)
ammonium molybdophosphate–polyacrylonitrile	15.8	Not measured	Park et al. (2010)
Synthetic hydroxyapatite	2.37	Not measured	Nishiyama et al. (2016)
Salvadora persica (Miswak) root powder	41.5	60	Hassan et al. (2020)
Biochar from pomelo peel	26.6	60	Guo et al. (2022)

Data availability

Data will be made available on request.

Acknowledgements

This work was originally supported by the Engineering and Physical Sciences Research Council through the UK Korea Civil Nuclear Energy program grant EP/M026558/1 Silicate Nanoparticles for Extraction of Radionuclides (SINNER).

References

Agency, N.E., 2018. State-of-the-art Report on the Progress of Nuclear Fuel Cycle Chemistry. Paris.

Aguila, B., Banerjee, D., Nie, Z.M., Shin, Y., Ma, S.Q., Thallapally, P.K., 2016. Selective removal of cesium and strontium using porous frameworks from high level nuclear waste. Chem. Commun. 52 (35), 5940–5942. https://doi.org/10.1039/c6cc00843g.

Al-Amrani, W.A., Hanafiah, M., Mohammed, A.H.A., 2022. A comprehensive review of anionic azo dyes adsorption on surface-functionalised silicas. Environ. Sci. Pollut. Control Ser. 29 (51), 76565–76610. https://doi.org/10.1007/s11356-022-23062-0. Nov.

Alamdarlo, F.V., Solookinejad, G., Zahakifar, F., Jalal, M.R., Jabbari, M., 2021. Study of kinetic, thermodynamic, and isotherm of Sr adsorption from aqueous solutions on graphene oxide (GO) and (aminomethyl)phosphonic acid-graphene oxide (AMPA-GO). J. Radioanal. Nucl. Chem. 329 (2), 1033–1043. https://doi.org/10.1007/s10967-021-07845-2. Aug.

Ali, S.A., Kazi, I.W., Ullah, N., 2015. New chelating ion-exchange resin synthesized via the cyclopolymerization protocol and its uptake performance for metal ion removal. Ind. Eng. Chem. Res. 54 (40), 9689–9698. https://doi.org/10.1021/acs.iecr.5b02267. Oct.

Ali, M.M.S., Abdel-Galil, E.A., Hamed, M.M., 2020. Removal of strontium radionuclides from liquid scintillation waste and environmental water samples. Appl. Radiat. Isot. 166, 109357. https://doi.org/10.1016/j.apradiso.2020.109357. Dec.

Amphlett, J.T.M., Ogden, M.D., Foster, R.I., Syna, N., Soldenhoff, K., Sharrad, C.A., 2018a. Polyamine functionalised ion exchange resins: synthesis, characterisation and uranyl uptake. Chem. Eng. J. 334, 1361–1370. https://doi.org/10.1016/j.cej.2017.11.040.

Amphlett, J.T.M., Sharrad, C.A., Foster, R.I., Ogden, M.D., 2018b. Ethylenediamine functionalised ion exchange resin for uranium recovery from acidic mixed sulfate-chloride media: initial column loading studies. Journal of the Southern African Institute of Mining and Metallurgy 118, 1521–1527.

Arcis, H., Zimmerman, G.H., Tremaine, P.R., 2014. Ion-pair formation in aqueous strontium chloride and strontium hydroxide solutions under hydrothermal conditions by AC conductivity measurements. Phys. Chem. Chem. Phys. 16 (33), 17688–17704. https://doi.org/10.1039/c4cp01703j. Sep.

Asmussen, R.M., Turner, J., Chong, S.H., Riley, B.J., 2022. Review of recent developments in iodine wasteform production. Front. Chem. 10, 1043653. https://doi.org/10.3389/fchem.2022.1043653. Dec.

C.M. Atkinson , G.D. Walker , T.J. Robshaw , M.J.D. Rushton , S.C. Middleburgh , and M. D. Ogden, "Optioneering in nuclear ion exchange resin disposal," Prog. Nucl. Energy, (in-press). doi: 10.2139/ssrn.4821025.

Barton, D.N.T., et al., 2019. Remediation of radioiodine using polyamine anion exchange resins. J. Ind. Eng. Chem. 78, 210–221.

Bezhin, N.A., Dovhyi, I.I., Tokar, E.A., Tananaev, I.G., 2021. Physical and chemical regularities of cesium and strontium recovery from the seawater by sorbents of various types. J. Radioanal. Nucl. Chem. 330 (3), 1101–1111. https://doi.org/10.1007/s10967-021-08027-w. Dec.

Bezzina, J.P., Robshaw, T., Dawson, R., Ogden, M.D., 2020. Single metal isotherm study of the ion exchange removal of Cu(II), Fe(II), Pb (II) and Zn(II) from synthetic acetic acid leachate. Aug Chem. Eng. J. 394, 124862–124872. https://doi.org/10.1016/j.cej.2020.124862. Art no. 124862.

Billo, E.J., 2004. Excel for Chemists: A Comprehensive Guide, 3 ed. John Wiley, Hoboken, New Jersey.

Bortun, A.I., Bortun, L.N., Clearfield, A., 1997. Evaluation of synthetic inorganic ion exchangers for cesium and strontium removal from contaminated groundwater and wastewater. Solvent Extr. Ion Exch. 15 (5), 909–929. https://doi.org/10.1080/07366299708934513.

Chiarizia, R., Horwitz, E.P., Beauvais, R.A., Alexandratos, S.D., 1998. Diphonix-CS: a novel combined cesium and strontium selective ion exchange resin. Solvent Extr. Ion Exch. 16 (3), 875–898. https://doi.org/10.1080/07366299808934558.

Cicero-Herman, C.A., Workman, P., Poole, K., Erich, D., Harden, J., 1998. Commercial Ion Exchange Vitrification in Borosilicate Glass. United States Department of Energy, Springfield, VA.

Da'na, E., 2017. Adsorption of heavy metals on functionalized-mesoporous silica: a review. Microporous Mesoporous Mater. 247, 145–157. https://doi.org/10.1016/j.micromeso.2017.03.050. Jul.

Dhami, P.S., et al., 2013. Separation and purification of ^{90}Sr from PUREX HLLW using *N*,*N*,*N*′,*N*′-tetra(2-ethylhexyl) diglycolamide. J. Radioanal. Nucl. Chem. 296 (3), 1341–1347. https://doi.org/10.1007/s10967-012-2302-0. Jun.

Doudou, S., et al., 2013. Optimised management of orphan wastes in the UK. Asme 2013 15th International Conference on Environmental Remediation and Radioactive Waste Management, Vol 1: Low/Intermediate-Level Radioactive Waste Management; Spent Fuel, Fissile Material, Transuranic and High-Level Radioactive Waste Management. https://doi.org/10.1115/icem2013-96330.

Dyer, A., Pillinger, M., Amin, S., 1999. Ion exchange of caesium and strontium on a titanosilicate analogue of the mineral pharmacosiderite. J. Mater. Chem. 9 (10), 2481–2487. https://doi.org/10.1039/a905549e. Oct.

Elma, M., Yacou, C., Wang, D.K., Smart, S., da Costa, J.C.D., 2012. Microporous silica based membranes for desalination. Water 4 (3), 629–649. https://doi.org/10.3390/w4030629. Sep.

Gin, S., et al., 2013. An international initiative on long-term behavior of high-level nuclear waste glass. Mater. Today 16 (6), 243–248. https://doi.org/10.1016/j.mattod.2013.06.008. Jun.

Guo, Y.X., et al., 2022. Strontium ion removal from artificial seawater using a combination of adsorption with biochar and precipitation by blowing CO_2 nanobubble with neutralization. Front. Bioeng. Biotechnol. 10. https://doi.org/10.3389/fbioe.2022.819407. Feb Art no. 819407.

Harland, C.E., 1994. Ion Exchange: Theory and Practice, second ed. Royal Society of Chemistry, Cambridge.

Harrison, J.D., Oatway, W.B., Brown, I.K., Hopewell, J.W., 2023. Health risks from radioactive particles on Cumbrian beaches near the Sellafield nuclear site. J. Radiol. Prot. 43 (3), 031504. https://doi.org/10.1088/1361-6498/acdfd6. Sep.

Hasegawa, Y., Maki, K., Sekine, T., 1967. Studies of the alkaline earth complexes in various solutions. III. Calcium(II) and strontium(II) complexes with sulfate and oxalate ions in 1M perchlorate media. Bull. Chem. Soc. Jpn. 40, 1845–1848.

Hassan, S.S.M., Kamel, A.H., Youssef, M.A., Aboterika, A.H.A., Awwad, N.S., 2020. Removal of barium and strontium from wastewater and radioactive wastes using a green bioadsorbent, *Salvadora persica* (Miswak). Desalination Water Treat. 192, 306–314. https://doi.org/10.5004/dwt.2020.25774. Jul.

James, A.M., Harding, S., Robshaw, T., Bramall, N., Ogden, M.D., Dawson, R., 2019. Selective environmental remediation of strontium and cesium using sulfonated hyper-cross-linked polymers (SHCPs). Applied Materials and Interfaces 11, 22464–22473.

Jantzen, C.M., Peeler, D.K., Cicero, C.A., 1995. Vitrification of Ion-Exchange (IEX) Resins: Advantages and Technical Challenges. International Atomic Energy Agency, Aiken, South Carolina.

Kalal, H.S., Khanchi, A.R., Nejatlabbaf, M., Almasian, M.R., Saberyan, K., Taghiof, M., 2017. The adsorption-desorption behavior of strontium ions with an impregnated resin containing di (2-ethylhexyl) phosphoric acid in aqueous solutions. Advances in Environmental Research-an International Journal 6 (4), 301–315. https://doi.org/10.12989/aer.2017.6.4.301. Dec.

Kaspar, T.C., et al., 2019. Physical and optical properties of the international simple glass. Apr npj Mater. Degrad. 3 (1). https://doi.org/10.1038/s41529-019-0069-2. Art no. 15.

Khanchi, A.R., Yavari, R., Pourazarsa, S.K., 2007. Preparation and evaluation of composite ion-exchanger for the removal of cesium and strontium radioisotopes. J. Radioanal. Nucl. Chem. 273 (1), 141–145. https://doi.org/10.1007/s10967-007-0725-9. Jul.

Kim, T., Kim, M., Jung, S.H., Yeon, J.W., 2018. Mitigation of radionuclide deposition in contaminated water: effects of pH on coprecipitation of Cs(I) and Sr(II) with Fe(III) in aqueous solutions. J. Radioanal. Nucl. Chem. 316 (3), 1261–1266. https://doi.org/10.1007/s10967-018-5828-y. Jun.

Labunska, I., et al., 2021. Current radiological situation in areas of Ukraine contaminated by the Chornobyl accident: Part 2. Strontium-90 transfer to culinary grains and forest woods from soils of Ivankiv district. Environ. Int. 146, 106282. https://doi.org/10.1016/j.envint.2020.106282. Jan.

Lanxess. "Product Information: Lewatit TP260." https://www.lenntech.com/Data-sheets/Lewatit-TP-260-L.pdf (accessed 13 August 2024).

Lennemann, W.L., 1978. The management of high-level radioactive wastes. IAEA 21.

Luttrell, G.H., More, C., Kenner, C.T., 1971. Effect of pH and ionic strength on ion exchange and chelating properties of an iminodiacetate ion exchange resin with alkaline earth ions. Anal. Chem. 43 (11), 1370. https://doi.org/10.1021/ac60305a048. &.

Management, C.o.R.W., 2023. CoRWM Report: Progress towards the Delivery of an Operational GDF. CoRWM.

Mason, C.F.V., Lu, N., Conca, J., 2000. Radioactive strontium- and caesium-contaminated sites: characterisation, transport, and remedial options. Nuclear Physical Methods in Radioecological Investigations of Nuclear Test Sites 31, 89–97.

Meyers, P.S., 1998. How chelating resins behave. In: Presented at the AESF/EPA Conference. Orlando, Florida.

Morisawa, S., Kitou, M., Shimada, Y., Yoneda, M., 2000. Evaluation of fallout strontium-90 accumulation in bone and cancer mortality risk in Japanese. J. Atom. Energy Soc. Jpn. 42 (9), 951–959. https://doi.org/10.3327/jaesj.42.951. Sep.

Nishiyama, Y., Hanafusa, T., Yamashita, J., Yamamoto, Y., Ono, T., 2016. Adsorption and removal of strontium in aqueous solution by synthetic hydroxyapatite. J. Radioanal. Nucl. Chem. 307 (2), 1279–1285. https://doi.org/10.1007/s10967-015-4228-9. Feb.

Ogden, M.D., Moon, E.M., Wilson, A., Pepper, S.E., 2017. Application of chelating weak base resin Dowex M4195 to the recovery of uranium from mixed sulfate/chloride media. Chem. Eng. J. 317, 80–89. https://doi.org/10.1016/j.cej.2017.02.041 (in English) Jun.

Oji, L.N., Martin, K.B., Hobbs, D.T., 2009. Development of prototype titanate ion-exchange loaded-membranes for strontium, cesium and actinide decontamination from aqueous media. J. Radioanal. Nucl. Chem. 279 (3), 847–854. https://doi.org/10.1007/s10967-008-7365-6. Mar.

Paasikallio, A., Rantavaara, A., Sippola, J., 1994. The transfer of Cesium-137 and Strontium-90 from soil to food crops after the Chernobyl accident. Sci. Total Environ. 155 (2), 109–124. https://doi.org/10.1016/0048-9697(94)90285-2. Oct.

Park, Y., Lee, Y.C., Shin, W.S., Choi, S.J., 2010. Removal of cobalt, strontium and cesium from radioactive laundry wastewater by ammonium molybdophosphate-polyacrylonitrile (AMP-PAN). Chem. Eng. J. 162 (2), 685–695. https://doi.org/10.1016/j.cej.2010.06.026. Aug.

Pepper, S.E., Whittle, K.R., Harwood, L.M., Cowell, J., Lee, T.S., Ogden, M.D., 2018. Cobalt and nickel uptake by silica-based extractants. Separ. Sci. Technol. 53 (10), 1552–1562. https://doi.org/10.1080/01496395.2017.1405034.

Pioch, M., Madozescande, C., 1995. Effect of rainwater on the remobilization and dissolution OF CS-134 and SR-85 contained in aerosols similar to those discharged in a nuclear accident and deposited in an urban-environment. J. Environ. Radioact. 26 (1), 51–61. https://doi.org/10.1016/0265-931x(95)91632-e.

Potera, C., 2011. Hazardous waste: pond algae sequester strontium-90. Environmental Health Perspectives 119, A244.

Povinec, P.P., Hirose, K., Aoyama, M., 2012. Radiostrontium in the western north pacific: characteristics, behavior, and the Fukushima impact. Environmental Science & Technology 46 (18), 10356–10363. https://doi.org/10.1021/es301997c. Sep.

Rapaport, H.I.E., Nikolic-Hughes, I., Hughes, E.W., 2022. Initial Strontium-90 concentrations in ocean sediment from the northern Marshall Islands. Journal of Radiation Research and Applied Sciences 15 (1), 17–20. https://doi.org/10.1016/j.jrras.2021.11.001. Mar.

Robshaw, T.J., 2019. Hydrometallurgical Remediation of Toxic Spent Potlining (SPL) Aluminium Waste for Conservation of Fluoride. University of Sheffield. PhD, Chemical and Biological Engineering.

Robshaw, T.J., Dawson, R., Bonser, K., Ogden, M.D., 2019a. Towards the implementation of an ion-exchange system for recovery of fluoride commodity chemicals. Kinetic and dynamic studies. Chem. Eng. J. 367, 149–159.

Robshaw, T., Tukra, S., Hammond, D.B., Leggett, G.J., Ogden, M.D., 2019b. Highly efficient fluoride extraction from simulant leachate of spent potlining via La-loaded chelating resin. An equilibrium study. J. Hazard Mater. 361, 200–209.

Robshaw, T.J., et al., 2020a. Insights into the interaction of iodide and iodine with Cu (II)-loaded bispicolylamine chelating resin and applications for nuclear waste treatment. Chem. Eng. J. 390, 124647–124659.

Robshaw, T.J., James, A.M., Hammond, D.B., Reynolds, J., Dawson, R., Ogden, M.D., 2020b. Calcium-loaded hydrophilic hypercrosslinked polymers for extremely high defluoridation capacity via multiple uptake mechanisms. J. Mater. Chem. A 8, 7130–7144.

Robshaw, T.J., Bonser, K., Coxhill, G., Dawson, R., Ogden, M.D., 2020c. Development of a combined leaching and ion-exchange system for valorisation of spent potlining waste. Waste and Biomass Valorization 11, 5467–5481.

Robshaw, T.J., Turner, J., Kearney, S., Walkley, B., Sharrad, C.A., Ogden, M.D., 2021. Capture of aqueous radioiodine species by metallated adsorbents from wastestreams of the nuclear power industry: a review. SN Appl. Sci. 3 (11). https://doi.org/10.1007/s42452-021-04818-8. Nov Art no. 843.

Robshaw, T.J., et al., 2023. Radioiodine abatement – development of radioiodine targeting strategies in the light of Zero emission. Prog. Nucl. Energy 165.

Sarkar, A.R., Datta, P.K., Sarkar, M., 1996. Sorption recovery of metal ions using silica gel modified with salicylaldoxime. Talanta 43 (11), 1857–1862. https://doi.org/10.1016/0039-9140(96)01953-4. Nov.

Shagina, N.B., Tolstykh, E.I., Fell, T.P., Smith, T.J., Harrison, J.D., Degteva, M.O., 2015. Strontium biokinetic model for the lactating woman and transfer to breast milk: application to Techa River studies. J. Radiol. Prot. 35 (3), 677–694. https://doi.org/10.1088/0952-4746/35/3/677. Sep.

Steinhauser, G., 2014. Fukushima's forgotten radionuclides: a review of the understudied radioactive emissions. Environmental Science & Technology 48 (9), 4649–4663. https://doi.org/10.1021/es405654c. May.

Strachan, D.M., Schulz, W.W., 1977. Vitrification of Strontium-90 Fluoride. Richland, WA.

Surman, J.J., Pates, J.M., Zhang, H., Happel, S., 2014. Development and characterisation of a new Sr selective resin for the rapid determination of Sr-90 in environmental water samples. Talanta 129, 623–628. https://doi.org/10.1016/j.talanta.2014.06.041. Nov.

Tan, S.H., Chen, X.G., Ye, Y., Sun, J., Dai, L.Q., Ding, Q., 2010. Hydrothermal removal of Sr^{2+} in aqueous solution via formation of Sr-substituted hydroxyapatite. J. Hazard Mater. 179 (1–3), 559–563. https://doi.org/10.1016/j.jhazmat.2010.03.040. Jul.

Tavakoli, H., Sepehrian, H., Semnani, F., Samadfam, M., 2013. Recovery of uranium from UCF liquid waste by anion exchange resin CG-400: breakthrough curves, elution behavior and modeling studies. Ann. Nucl. Energy 54, 149–153. https://doi.org/10.1016/j.anucene.2012.11.012 (in English) Apr.

Tazoe, H., et al., 2019. Observation of dispersion in the Japanese coastal area of released ^{90}Sr, ^{134}Cs, and ^{137}Cs from the Fukushima Daiichi nuclear power plant to the sea in 2013. Int. J. Environ. Res. Publ. Health 16 (21), 4094. https://doi.org/10.3390/ijerph16214094. Nov.

Tran, H.N., You, S.J., Hosseini-Bandegharaei, A., Chao, H.P., 2017. Mistakes and inconsistencies regarding adsorption of contaminants from aqueous solutions: a critical review. Water Res. 120, 88–116. https://doi.org/10.1016/j.watres.2017.04.014. Sep.

Vajda, N., Kim, C.K., 2010. Determination of radiostrontium isotopes: a review of analytical methodology. Appl. Radiat. Isot. 68 (12), 2306–2326. https://doi.org/10.1016/j.apradiso.2010.05.013.

Vidal, L., Parshintsev, J., Hartonen, K., Canals, A., Riekkola, M.L., 2012. Ionic liquid-functionalized silica for selective solid-phase extraction of organic acids, amines and aldehydes. J. Chromatogr. A 1226, 2–10. https://doi.org/10.1016/j.chroma.2011.08.075. Feb.

Wu, D.B., Sun, Y.H., Wang, Q.G., 2013. Adsorption of lanthanum (III) from aqueous solution using 2-ethylhexyl phosphonic acid mono-2-ethylhexyl ester-grafted magnetic silica nanocomposites. J. Hazard Mater. 260, 409–419. https://doi.org/10.1016/j.jhazmat.2013.05.042. Sep.

Wu, L.Y., Zhang, G.H., Wang, Q.Z., Hou, L., Gu, P., 2014. Removal of strontium from liquid waste using a hydraulic pellet co-precipitation microfiltration (HPC-MF) process. Desalination 349, 31–38. https://doi.org/10.1016/j.desal.2014.06.020. Sep.

Zhang, W., He, X.H., Ye, G., Yi, R., Chen, J., 2014. Americium(III) capture using phosphonic acid-functionalized silicas with different mesoporous morphologies: adsorption behavior study and mechanism investigation by EXAFS/XPS. Environmental Science & Technology 48 (12), 6874–6881. https://doi.org/10.1021/es500563q. Jun.

Zhou, L.M., et al., 2016. Adsorption of uranium(VI) from aqueous solution using phosphonic acid-functionalized silica magnetic microspheres. J. Radioanal. Nucl. Chem. 310 (3), 1155–1163. https://doi.org/10.1007/s10967-016-4878-2. Dec.